IOP Publishing Plasma Physics and Controlled Fusion

Plasma Phys. Control. Fusion **56** (2014) 035005 (11pp) doi:10.1088/0741-3335/56/3/035005

Linear ideal MHD predictions for $n = 2$ non-axisymmetric magnetic perturbations on DIII-D

S R Haskey[1], M J Lanctot[2], Y Q Liu[3], J M Hanson[4], B D Blackwell[1] and R Nazikian[5]

[1] Plasma Research Laboratory, Research School of Physics and Engineering, The Australian National University, Canberra, ACT 0200, Australia
[2] General Atomics, PO Box 85806, San Diego, CA 92186-5608, USA
[3] Euratom/CCFE Fusion Association, Culham Science Centre, Abingdon, OX14 3DB, UK
[4] Columbia University, 116th St and Broadway, New York, NY 10027, USA
[5] Princeton Plasma Physics Laboratory, Princeton, NJ 08543-0451, USA

E-mail: shaun.haskey@anu.edu.au

Received 25 July 2013, revised 20 December 2013
Accepted for publication 14 January 2014
Published 5 February 2014

Abstract

An extensive examination of the plasma response to dominantly $n = 2$ non-axisymmetric magnetic perturbations (MPs) on the DIII-D tokamak shows the potential to control 3D field interactions by varying the poloidal spectrum of the radial magnetic field. The plasma response is calculated as a function of the applied magnetic field structure and plasma parameters, using the linear magnetohydrodynamic code MARS-F (Liu *et al* 2000 *Phys. Plasmas* **7** 3681). The ideal, single fluid plasma response is decomposed into two main components: a local pitch-resonant response occurring at rational magnetic flux surfaces, and a global kink response. The efficiency with which the field couples to the total plasma response is determined by the safety factor and the structure of the applied field. In many cases, control of the applied field has a more significant effect than control of plasma parameters, which is of particular interest since it can be modified at will throughout a shot to achieve a desired effect. The presence of toroidal harmonics, other than the dominant $n = 2$ component, is examined revealing a significant $n = 4$ component in the perturbations applied by the DIII-D MP coils; however, modeling shows the plasma responses to $n = 4$ perturbations are substantially smaller than the dominant $n = 2$ responses in most situations.

Keywords: edge localized modes, resonant magnetic perturbations, magnetohydrodynamics, tokamaks, toroidal plasma confinement

(Some figures may appear in colour only in the online journal)

1. Introduction

Non-axisymmetric magnetic perturbations (MPs) have been used on tokamaks to suppress [1–5], mitigate [6, 7] and destabilize [8] edge-localized modes (ELMs), perform magnetic spectroscopy [9, 10], control resistive wall modes [11, 12] and neoclassical tearing modes [13], and correct error fields [14, 15]. Due to their role in accessing fusion relevant plasma scenarios, perturbation coil sets are now an integral system on many major tokamaks [16, 17]. Recently, ELM suppression using dominantly $n = 2$ perturbations has been achieved on DIII-D, which was previously only attainable using $n = 3$ fields [18]. The suppression was achieved using the internal coils (I-coils), two rows of six coils each, located above and below the midplane inside the vacuum vessel. ELM suppression was found within different ranges of safety factors depending on the structure of the applied field, with suppression occurring for applied fields found to couple best to marginally stable kink modes. Additionally, the $n = 2$ configuration on DIII-D offers substantially more control over the applied poloidal spectrum of the radial magnetic field than $n = 3$ and as such, has been the focus of recent experiments

[18]. These results have motivated an extensive examination of the $n = 2$ plasma response in DIII-D equilibria over a wide range of plasma parameters and applied fields. The results presented here are useful for guiding future experiments and for correlating the ideal plasma response with observed experimental outcomes.

A single coil produces a magnetic field with a radial component that is normal to the equilibrium magnetic flux surfaces. The radial component of the magnetic field can be Fourier decomposed along the toroidal and poloidal angles of the torus to produce a spectrum of toroidal (n) and poloidal (m) harmonics, hereafter referred to as the toroidal and poloidal spectra. These spectra are controlled by combining fields from multiple coils. The toroidal spectrum is controlled by the relative phase difference of the currents in coils at the same poloidal angle but different toroidal angles. Similarly, the poloidal spectrum is controlled by the relative phase difference of the currents in coils at the same toroidal angle but different poloidal angles. Here, we consider $n = 2$ fields, where the toroidal phase difference between currents in the upper and lower I-coil, $\Delta\phi_{\rm ul}$, is defined through the following relations: $I_{\rm upper} \propto \cos(n\phi_{\rm coil})$ and $I_{\rm lower} \propto \cos(n\phi_{\rm coil} + \Delta\phi_{\rm ul})$, where $I_{\rm upper}$ and $I_{\rm lower}$ are the currents in the MP coils above and below the midplane respectively, and $\phi_{\rm coil}$ is the DIII-D tokamak toroidal angle location of the center of a MP coil. The DIII-D tokamak toroidal angle is in the opposite direction to the toroidal equilibrium magnetic field.

Previous studies have found that the measured magnetic field is substantially different from that predicted in a pure vacuum case, indicating the need to take into account the plasma response in MP calculations. For example, in [19], the plasma response to an applied MP, as measured by a midplane poloidal pickup coil, normalized to the MP coil current, showed a strong dependence on $\beta_{\rm N} = \beta(\%)a(m)B_0(T)/I_{\rm p}({\rm MA})$, with the pickup output due to the plasma response exceeding the output of a radial pickup due to the vacuum field by more than a factor of 10 at high $\beta_{\rm N}$. Here, $\beta = 2\mu_0\langle p\rangle/B_0^2$, $\langle p\rangle$ represents the volume-averaged pressure, μ_0 the magnetic permeability of free space, $I_{\rm p}$ the plasma current, a the plasma minor radius and B_0 the equilibrium magnetic field strength on axis. This substantial modification of the magnetic field by the plasma indicates the importance of including the plasma response when modeling non-axisymmetric plasma equilibria.

Both screening and amplification can occur in the plasma response to MPs. The screening, at least in the linear (small-island) regime, robustly occurs for the resonant component of the MP, either due to an ideal plasma response or due to fast plasma flow. There is strong experimental evidence of screening, for example smaller lobe sizes than vacuum predictions in MAST, and the absence of strike point splitting in H-mode JET discharges [21]. The amplification, due to excitation of marginally stable modes (such as the kink mode) by the non-resonant components of the MP, depends on the equilibrium configuration, in particular on the plasma pressure. In order to model the plasma response within the framework of magnetohydrodynamic (MHD), one can follow the time-dependent dynamic evolution of the 2D equilibria until a 3D steady-state solution is reached, or one can attempt to find a nearby 3D equilibrium. Additionally, the problem can be treated linearly or non-linearly, leading to four different approaches [20].

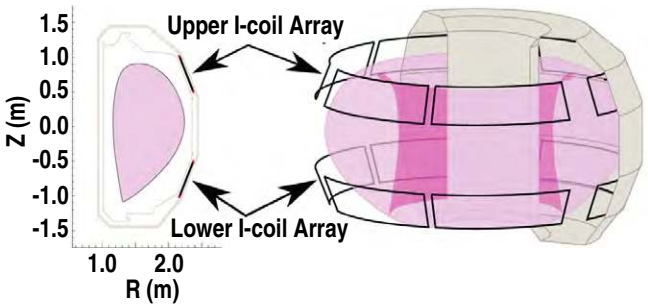

Figure 1. 3D picture showing the radial location of the I-coils with respect to the DIII-D vacuum vessel. Poloidal cross section shows the location of the I-coils above and below the midplane.

In this paper, we have used the single fluid linear MHD code MARS-F [22], which treats the 3D MP as a time-dependent, driven problem. This approach does not include non-linear effects, but can include a resistive wall, toroidal rotation, plasma resistivity, and guarantees force balance. In the simulations presented here, we include a resistive wall, but exclude plasma rotation and resistivity.

While there are non-linear codes such as M3D [23, 24], M3D-C^1 [25], NIMROD [26, 27], RMHD [28] or JOREK [29, 30], the linear approach has the significant advantage of being less computationally intensive and has been experimentally validated. For example, previous work looking at the $n = 1$ and 3 perturbations on DIII-D [19, 31] found good qualitative agreement between MARS-F predictions and measurements from the magnetic pickup coils up to 80% of the predicted ideal MHD pressure limit calculated without a conducting wall near the plasma edge ($\beta_{\rm N}^{\rm NW}$). At larger $\beta_{\rm N}$, the MARS-F code predicts a much larger plasma response, indicating the need to include additional physics, or non-linear effects.

This paper is organized as follows. In section 2, we introduce the MP coils on DIII-D and discuss the differences between the MARS-F coil representation and a geometrically accurate representation of the MP coils. Section 3 describes the main components of the ideal plasma response and how we separate and quantify these components. Section 4 presents maps showing the parameter dependence of the components described in section 3. These maps are particularly useful for guiding experiments, and some examples of their use is given. Lastly, section 5 considers the importance of harmonics other than the dominant $n = 2$ component.

2. Validation of the MARS-F MP coil representation

In this study, we consider the plasma response to fields applied with the I-coil. Half of the coils are located above the midplane, and the other half are below, as shown in figure 1. The six toroidal locations allow perturbations with dominant toroidal mode numbers up to 3 to be applied. Higher harmonics are also present due to the geometry of the I-coils as discussed below.

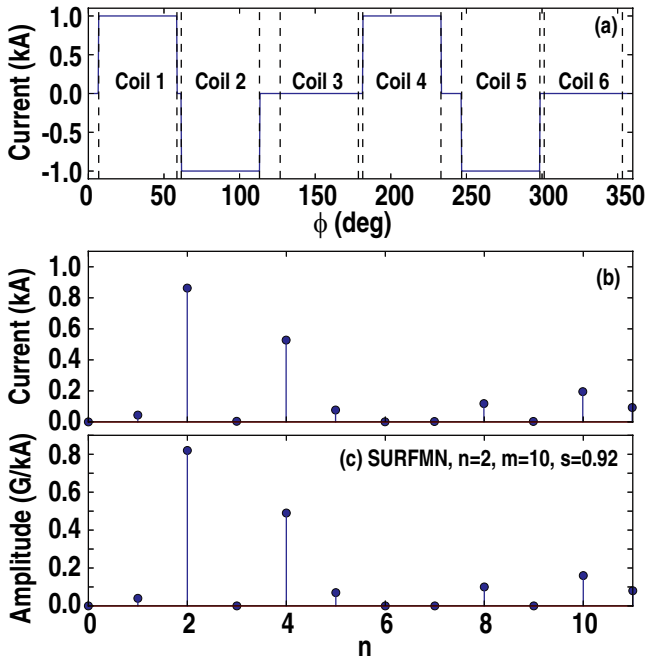

Figure 2. (*a*) A simplified picture of the magnetic field normal to the midpoint of the upper (or lower) I-coil array as a function of ϕ for a common $n = 2$ configuration on DIII-D (top). The toroidal extent of each of the coils in the array is marked by the dashed vertical lines. (*b*) Fourier decomposition of this profile in the toroidal direction shows that in addition to the dominant $n = 2$ component, there is a significant $n = 4$ component present. (*c*) The toroidal harmonic content of the $m = 10$ mode at $s = 0.92$ calculated using SURFMN showing the toroidal harmonics that are present in addition to $n = 2$.

Adjusting $\Delta\phi_{\rm ul}$ allows the poloidal harmonic (m) spectrum of the applied field to be modified. Refer to section 1 for the definition of $\Delta\phi_{\rm ul}$ as it is used in this paper.

As described in [32], MARS-F does not include the full 3D geometry of the MP coils. Instead, the source current, $\boldsymbol{j}_{\rm MP}$, is represented as a surface current at the radial location of the MP coils. The toroidal component of $\boldsymbol{j}_{\rm MP}$ has a finite width along the poloidal angle, similar to the pointwise MP coil current on the poloidal plane, and varies as $\exp(in\phi)$ along the toroidal angle, ϕ. The poloidal component of $\boldsymbol{j}_{\rm MP}$ is obtained from the divergence-free condition ($\nabla \cdot \boldsymbol{j}_{\rm MP} = 0$) and the MP field generated by $\boldsymbol{j}_{\rm MP}$ is determined by $\nabla \times \boldsymbol{b} = \boldsymbol{j}_{\rm MP}$.

In order to quantitatively compare MARS-F calculations with experiment, it is necessary to calculate the equivalent amplitude of the applied field in the simple coil model. The mapping employed is illustrated in figure 2(*a*) where the simplified magnetic field normal to the midpoint of the upper (or lower) I-coil array is plotted as a function of toroidal angle ϕ for a common $n = 2$ configuration on DIII-D. Fourier decomposition of this simplified field profile shows that a significant $n = 4$ component is present in addition to the dominant $n = 2$ component (figure 2(*b*)). While this is a simplistic treatment, it allows us to estimate an approximately equivalent $n = 2$ current for MARS-F in order to compare with experiments and vacuum codes. In this case, using figure 2(*b*), we set the MARS-F equivalent $n = 2$ current to 0.86 times the maximum current in the I-coils. The presence of harmonics other than $n = 2$ is discussed later in this section.

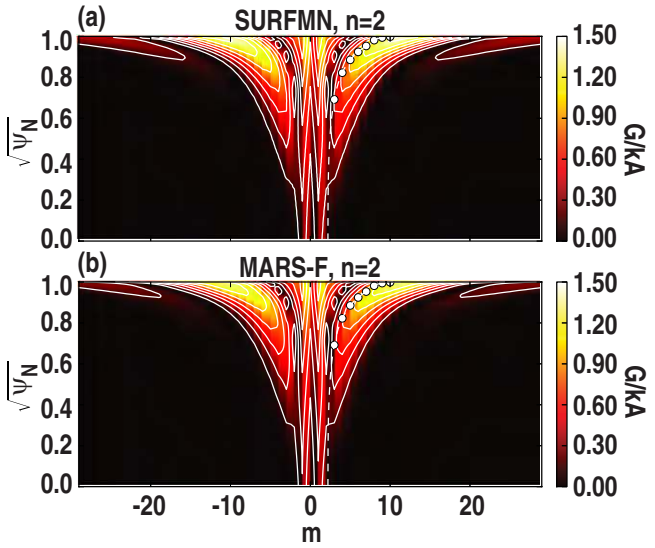

Figure 3. Poloidal harmonic content of the applied field calculated using SURFMN (*a*) and MARS-F (*b*) for the $n = 2$ component of the dominantly $n = 2$ MP. The locus of pitch resonance ($m = nq$) for a particular equilibrium with $q_{95} = 3.9$, is overlaid with the location of low order pitch-resonant harmonics marked with a dot. The MARS-F and SURFMN harmonic structures are in good agreement.

To assess the accuracy of the $n = 2$ applied vacuum field from MARS-F, we compare it with the output from the SURFMN vacuum code [33], which includes a realistic geometric model of the I-coils. Here, we Fourier decompose the magnetic field normal to the flux surfaces in the toroidal and poloidal directions in straight field line coordinates, as described in appendix A of [33], to obtain $\delta B_r^{m,n}(s)$, where m and n represent the poloidal and toroidal harmonics respectively, $s = \sqrt{\psi_{\rm N}}$ is a flux surface label and $\psi_{\rm N}$ is the normalized poloidal flux. In addition, we can define $\delta B_{r,\rm vac}^{m,n}(s)$, $\delta B_{r,\rm plas}^{m,n}(s)$, and $\delta B_{r,\rm tot}^{m,n}(s) = \delta B_{r,\rm vac}^{m,n}(s) + \delta B_{r,\rm plas}^{m,n}(s)$ where $\delta B_{r,\rm vac}^{m,n}$ is the field generated by the MP coils, $\delta B_{r,\rm plas}^{m,n}$ is the plasma generated field and $\delta B_{r,\rm tot}^{m,n}$ is the sum of the two. Each of these fields is normalized to the MP coil current and is reported in units of $\mathrm{G\,kA^{-1}}$.

The toroidal spectrum of the applied field calculated with SURFMN shows significant toroidal sidebands. The toroidal harmonic amplitudes for the magnetic field normal to the flux surfaces for the $m = 10$ component at $s = 0.92$ [$|\delta B_{r,\rm vac}^{m=10,n}(s = 0.92)|$] calculated by SURFMN for the $\Delta\phi_{\rm ul} = 0^\circ$ case are shown in figure 2(*c*). We choose $m = 10$ and $s = 0.92$ for this comparison because these values are in the range of interest in later sections of this paper. As expected, the $n = 2$ component is the largest; however, there are significant contributions from other toroidal harmonics, in particular $n = 4$. Comparing figure 2(*c*) with figure 2(*b*), we see that the simplistic model provides a good estimate of the relative amplitude of the different toroidal harmonics.

There is good agreement between SURFMN and MARS-F for the poloidal harmonic structure of the $n = 2$ toroidal harmonic. A comparison between SURFMN and MARS-F for the $|\delta B_{r,\rm vac}^{m,n=2}(s)|$ harmonics for $\Delta\phi_{\rm ul} = 0^\circ$ is shown in figure 3. For clarity, the radial dependence of some individual

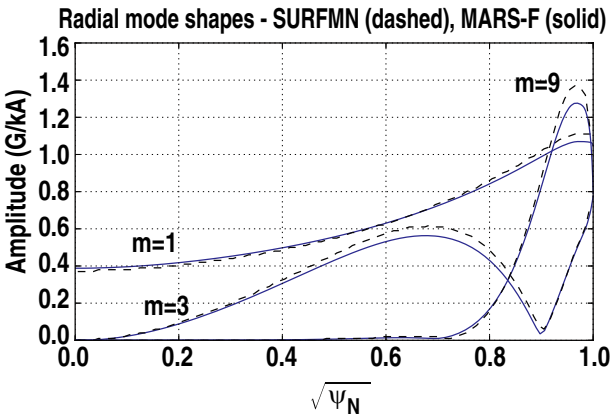

Figure 4. Comparison between the radial structure of selected vacuum poloidal harmonics calculated by SURFMN (dashed) and MARS-F (solid) for $n = 2$, showing good agreement.

poloidal harmonics is shown in figure 4. For this comparison, we set the MARS-F MP current to the $n = 2$ component shown in figure 2(b). In the plasma volume, the MARS-F model is in quantitative agreement with SURFMN to within ≈8%.

A comparison between SURFMN and MARS-F for the $|\delta B^{m,n=4}_{r,\mathrm{vac}}(s)|$ harmonics for $\Delta\phi_{\mathrm{ul}} = 0^\circ$ is shown in figure 5, with the MARS-F MP current set to the $n = 4$ component shown in figure 2(b). As with the $n = 2$ harmonic, the agreement between the two codes is good suggesting MARS-F can accurately model the individual toroidal harmonics of the I-coil MP.

The presence of toroidal harmonics other than $n = 2$ can be taken into account in MARS-F by performing separate simulations for each harmonic, while accounting for the relative strength of each harmonic in the vacuum field (figure 2(b)). In section 5, we will show that the $n = 4$ plasma response is negligible, except in some special circumstances.

3. Components of the ideal MHD plasma response

The scope of this paper is limited to the ideal MHD plasma response. The effects of resistivity and rotation are the subject of future work. The plasma response, $\delta B^{m,n}_{r,\mathrm{plas}}(s)$, consists of two main components in the ideal MHD case for the low frequency/static, low-n fields, applied by the I-coils. Firstly, there is a screening of the magnetic field normal to the flux surfaces, which occurs for magnetic field line pitch-resonant harmonics $m = nq$ (hereafter referred to as pitch-resonant component of the response). Secondly, there is a coupling to the stable external kink mode, which generally occurs for poloidal harmonics $nq < m < 3nq$ (hereafter referred to as kink-resonant component [34]). The location of these harmonics in the poloidal spectrum of the plasma response to the $n = 2$ component of the MP [$|\delta B^{m,n=2}_{r,\mathrm{plas}}(s)|$] are shown in figure 6, along with $|\delta B^{m,n=2}_{r,\mathrm{vac}}(s)|$ and $|\delta B^{m,n=2}_{r,\mathrm{tot}}(s)|$.

Pitch-resonant fields are of interest due to their role in the creation of stochastic magnetic fields, which may reduce the edge pressure gradient below the ELM instability threshold [35]. In the ideal MHD model, the plasma responds to the pitch-resonant fields by generating currents, which reduce the

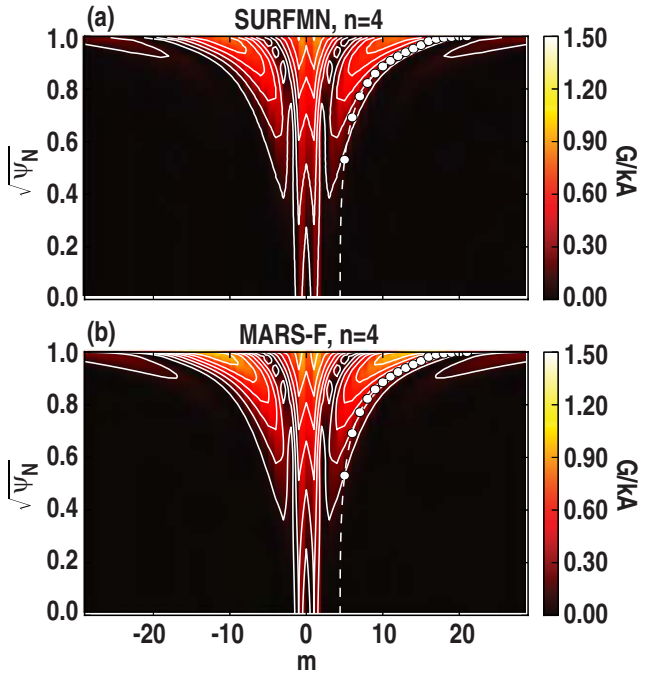

Figure 5. Poloidal harmonic content of the applied field as calculated using SURFMN (a) and MARS-F (b) for the $n = 4$ component of the dominantly $n = 2$ MP. The locus of pitch resonance ($m = nq$) for a particular equilibrium with $q_{95} = 3.9$, is overlaid with the location of low order pitch-resonant harmonics marked with a dot. As with the $n = 2$ harmonic, the MARS-F and SURFMN poloidal harmonic structures are in good agreement.

pitch-resonant components to zero [$\delta B^{m=nq,n}_{r,\mathrm{tot}}(s) = 0$], leaving the magnetic topology unchanged and preventing islands from forming near the rational surfaces. Pitch-resonant fields are also of interest because in the case where the islands are suppressed by plasma rotation, the resulting currents create an electromagnetic torque which acts as a sink in the toroidal momentum balance equation [36]. The cancellation of the fields at the pitch-resonant surfaces can be seen in figure 12. When plasma resistivity and toroidal rotation are taken into account, it is possible to amplify the pitch-resonant components for sufficiently slow rotation leading to larger islands than predicted by vacuum theory alone [32]. More generally, the pitch-resonant harmonics are subject to increased attenuation as the resistivity is decreased or the rotation is increased [32].

To quantify the degree of pitch-resonant drive, we calculate the sum of all the applied pitch-resonant harmonics in the vacuum field, and the average of all the applied pitch-resonant harmonics in the vacuum field (where N^n_{res} is the number of pitch-resonant harmonics satisfying $m = nq$ in the plasma):

$$\delta B^n_{\mathrm{res}} = \sum |\delta B^{m=nq,n}_{r,\mathrm{vac}}(s)|, \tag{1}$$

$$\overline{\delta B}^n_{\mathrm{res}} = \delta B^n_{\mathrm{res}} / N^n_{\mathrm{res}}. \tag{2}$$

It is useful to consider $\overline{\delta B}^n_{\mathrm{res}}$ as well as $\delta B^n_{\mathrm{res}}$ to capture the strength of the individual resonant harmonics in addition to the number of resonant harmonics, which increases

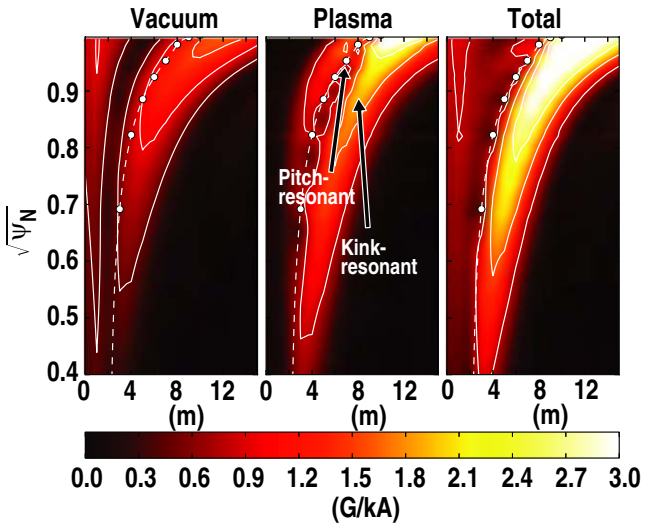

Figure 6. The amplitude of the vacuum, plasma and total $n = 2$ poloidal harmonics ($|\delta B^{m,n=2}_{r,\mathrm{vac}}(s)|$, $|\delta B^{m,n=2}_{r,\mathrm{plas}}(s)|$ and $|\delta B^{m,n=2}_{r,\mathrm{tot}}(s)|$) as calculated by MARS-F. The ideal plasma response has two main components, a pitch-resonant response, which acts to perfectly cancel the applied pitch-resonant field (harmonics $m = nq$) and an amplification of the harmonics that couple to the kink mode (poloidal harmonics satisfying $nq < m < 3nq$). The $m = nq$ line for the equilibrium used ($q_{95} = 3.9$ and $\beta_N/\ell_i = 2.0$) is overlaid with the location of low-order rational surfaces marked with a white dot. These images have been smoothed over the discrete m to make trends easier to see.

with q_{95}. The number of resonant harmonics is bounded for the equilibria used here because MARS-F requires a finite edge q. This is discussed in section 4.

For the pitch-resonant calculations, we do not take the ideal plasma response into account because it is equal and opposite to the applied vacuum field [$\delta B^{m=nq,n}_{r,\mathrm{plas}}(s) = -\delta B^{m=nq,n}_{r,\mathrm{vac}}(s)$]. While the formation of magnetic islands in the ideal plasma response case is not possible, these measures indicate how strongly the vacuum field couples to the pitch-resonant harmonics, and are still useful measures of the possibility of island formation when resistivity and rotation are considered. Including the effects of resistivity and rotation is outside the scope of this paper.

Poloidal harmonics in the range $nq < m < 3nq$ can couple to a stable external global kink mode, resulting in substantial amplification of these harmonics. This is often referred to as resonant field amplification (RFA) [37], and can be clearly seen in figures 6 and 12. The level to which the kink mode is driven is of interest for several reasons. Firstly the experimentally observed $n = 2$ ELM suppression windows in [18] correspond to upper–lower I-coil phasings that maximize the kink-resonant response. Also, a disruption may occur if the mode is driven to sufficiently large amplitude. Finally, the excitation of this mode can give rise to larger plasma displacements which generally apply a braking torque to the plasma through the increased neoclassical toroidal viscosity (NTV) [36]. The responses from other stable global modes (for example Alfvén eigenmodes, internal kink, tearing modes, ballooning modes) are not usually seen because they generally have higher n numbers, and/or high rotation frequency meaning they cannot be in direct resonance with the low-frequency/static, low-n MPs considered here [38]. These modes can interact non-linearly with the low-n MP, although it is not possible to see this interaction in the linear approach considered here. The effect of resistivity and rotation on the RFA as calculated using MARS-F are described in [38]. It was found that ideal and resistive plasma responses result in similar peak amplitudes for all poloidal harmonics, while decreases in rotation generally increase the RFA although this effect is reduced as plasma resistivity is decreased.

To quantify the extent of the coupling to the external kink mode, we find the strongest harmonic in the plasma response that is in the range $nq + 2 < m < 3nq$ at a particular flux surface near the edge of the plasma. This measure can be represented as follows:

$$\delta B^n_{\mathrm{kink}} = |\delta B^{m^*,n}_{r,\mathrm{plas}}(s = 0.92)|, \tag{3}$$

where m^* is the harmonic that gives the maximum plasma response for any $\Delta\phi_{\mathrm{ul}}$:

$$m^* = \arg\max_{nq+2<m<3nq} |\delta B^{m,n}_{r,\mathrm{plas}}(s = 0.92, \Delta\phi_{\mathrm{ul}})|. \tag{4}$$

We set the lower bound for m to be $nq + 2$ so that we avoid accidental selection of harmonics which may be part of the plasma screening response. Low-n peeling modes have also been observed for the low-frequency/static, low-n MPs [38], and as we will show in section 4.2, there is some evidence for excitation of these modes as a new pitch-resonant surface enters the plasma, although the extent to which this is introduced due to smoothing of the x-point (as required by MARS-F) is under investigation. The peeling response is captured as part of the $\delta B^n_{\mathrm{kink}}$ measure but is isolated to narrow q_{95} ranges.

4. Maps of the ideal plasma response sensitivity to upper–lower I-coil phasing and plasma equilibrium parameters

In this section, we explore the amplitudes of the pitch-resonant and kink-resonant responses as a function of $\Delta\phi_{\mathrm{ul}}$ and parameters such as plasma pressure and magnetic topology near the boundary. $\Delta\phi_{\mathrm{ul}}$ represents the toroidal phase difference between currents in the upper and lower I-coil, which determines the poloidal spectrum of the applied radial magnetic field. Kirk *et al* [39] examined ELM mitigation (as measured by the ELM frequency) on MAST as a function of many parameters including $\Delta\phi_{\mathrm{ul}}$ and q_{95}. A strong dependence was found for both of these parameters because they change the alignment of the applied perturbation (affected by $\Delta\phi_{\mathrm{ul}}$) with the pitch of the equilibrium magnetic field (affected by q_{95}). Given the relatively narrow poloidal extent of the coils on MAST and the fine control of $\Delta\Phi_{\mathrm{ul}}$ possible with 12 coils, we speculate that mapping out the parameter dependencies as described here may identify specific coil configurations that could be used to investigate the role of kink- and pitch-resonant harmonics in ELM mitigation on MAST. Unfortunately, on DIII-D, the upper and lower I-coil arrays consist of only six coils, making it impossible to make fine changes in the $n = 3$ poloidal spectrum with the I-coil alone. However,

by including $n = 3$ fields from another coil row such as the C-coil, it may be possible to vary the relative amplitudes of the kink- and pitch-resonant harmonics. This illustrates how mapping out these parameter dependencies is particularly useful for guiding experiments because it helps to identify important regions of parameter space, such as where island creation is more likely, or when coupling to the kink mode is optimized. This type of information can also be used in real-time control applications, such as changing $\Delta\phi_{ul}$ to maximize the resonant drive throughout a shot. We use $\delta B_{res}^{n=2}$ and $\overline{\delta B}_{res}^{n=2}$ to quantify the pitch-resonant response, and $\delta B_{kink}^{n=2}$ to quantify the kink-resonant response. The plasma pressure and magnetic topology are quantified using β_N/ℓ_i and q_{95} respectively (ℓ_i represents the plasma inductance).

Starting with a single experimental equilibrium reconstruction, the plasma pressure profile and safety factor profile were scaled and the equilibria solved by setting current as the free variable, to generate a set of ≈1000 equilibria, which form a well-sampled (β_N/ℓ_i, q_{95}) space. The pressure profile is scaled using a single multiplier, while the q profile is scaled so that q near the plasma edge is modified while q near the plasma center remains relatively unchanged. For each q-profile, the maximum pressure is chosen to be marginally below the $n = 2$ no-wall stability limit. We consider H-mode, lower single-null DIII-D scenarios, with ITER similar shape (ISS) as our initial equilibria. As with [31], the magnetic field pitch angle measurements from multiple motional Stark effect (MSE) polarimeters [40], kinetic profile measurements from Thomson scattering [41] and charge exchange recombination spectroscopy (CER) [42], and ONETWO [43] transport calculations of the total pressure, including the contribution from non-thermal beam ions, are used to constrain reconstructions of the axisymmetric magnetic field using the EFIT code [44].

Since the MARS-F calculation is performed in flux coordinates, it cannot treat the exact separatrix geometry. Therefore, the EFIT equilibria were truncated to include 99.7% of the total poloidal flux. Test cases with flux truncation between 99.0% and 99.7% showed the calculated plasma response was not sensitive to this parameter in this range of values. The pressure and q-profiles are then scaled and the equilibria solved by setting current as the free variable, using the Grad–Shafranov solver in the CORSICA code [45]. Examples of the scaled profiles are shown in figure 7, and the location of the equilibria in (β_N/ℓ_i, q_{95}) space is marked by black dots in figure 8. Figure 8 also marks the location of the $n = 2$ no-wall stability limit calculated using the DCON code [46]. The grid for MARS-F is created using the CHEASE code [47] and in the MARS-F calculations, a thin resistive axisymmetric shell is included to model the effect of the DIII-D wall.

4.1. Maps of the pitch-resonant response

The strength of the pitch-resonant drive depends strongly on $\Delta\phi_{ul}$ and the magnetic topology near the boundary (as measured by q_{95}), with a weaker dependence on plasma pressure (as measured by β_N/ℓ_i). Figure 8 shows $\delta B_{res}^{n=2}$ and $\overline{\delta B}_{res}^{n=2}$ (defined in equations (1) and (2)) calculated as

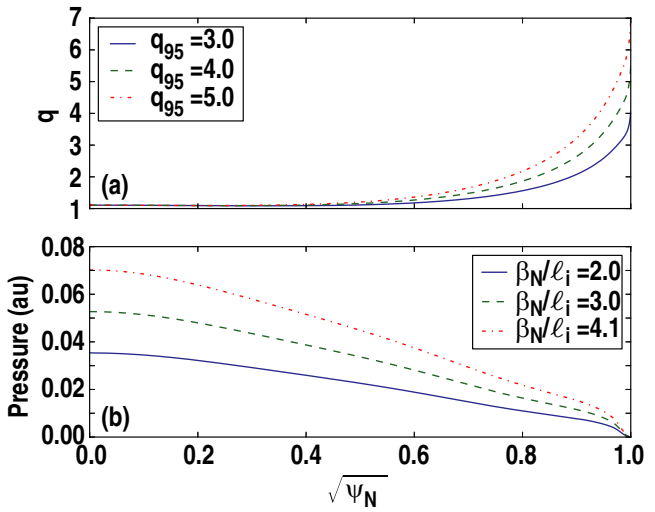

Figure 7. Examples of the scaled pressure (b) and q-profiles (a) that are used in the q_{95} and β_N/ℓ_i scans.

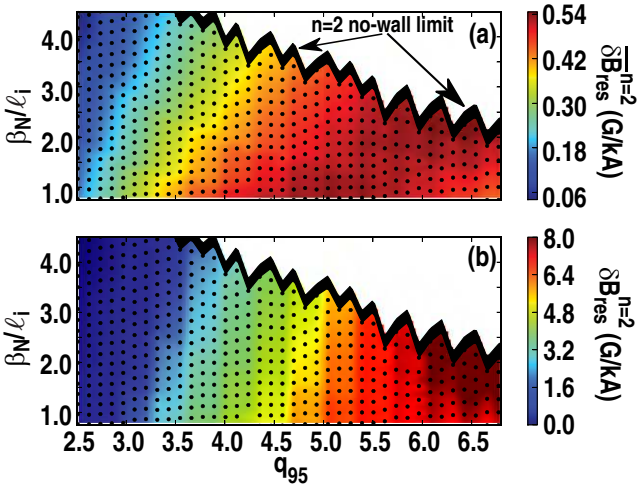

Figure 8. Measures of pitch-resonant drive, $\overline{\delta B}_{res}^{n=2}$ (a) and $\delta B_{res}^{n=2}$ (b) calculated as a function of β_N/ℓ_i and q_{95}, for $\Delta\phi_{ul} = 0°$, exhibiting a strong dependence on q_{95}, and a smaller dependence on β_N/ℓ_i. The β_N/ℓ_i and q_{95} dependence of $\delta B_{res}^{n=2}$ and $\overline{\delta B}_{res}^{n=2}$ are similar. The thick black line marks the $n = 2$ no-wall limit.

a function of these parameters for $\Delta\phi_{ul} = 0°$. The pitch-resonant drive depends predominantly on the location of the pitch-resonant line ($m = nq$) relative to the large amplitude lobes in $\delta B_{r,vac}^{m,n=2}(s)$ (as marked in figure 9). Changes in plasma pressure can modify the location of the flux surfaces relative to the applied field through the Shafranov shift; however, this effect is minimal compared to the dependence on q_{95} and $\Delta\phi_{ul}$. Comparing figures 8(a) and (b), we can see that $\delta B_{res}^{n=2}$ and $\overline{\delta B}_{res}^{n=2}$ produce similar results, although $\overline{\delta B}_{res}^{n=2}$ increases more rapidly at lower q_{95}, and $\delta B_{res}^{n=2}$ increases more rapidly at higher q_{95}. The reason these two measures are alike is because the shape of contours of constant amplitude in $\delta B_{r,vac}^{m,n=2}(s)$, follow a similar path in (s, m) space to the $m = nq$ line as shown in figures 6 and 9.

Varying $\Delta\phi_{ul}$ significantly alters the vacuum poloidal spectrum, which causes large variations in the pitch-resonant

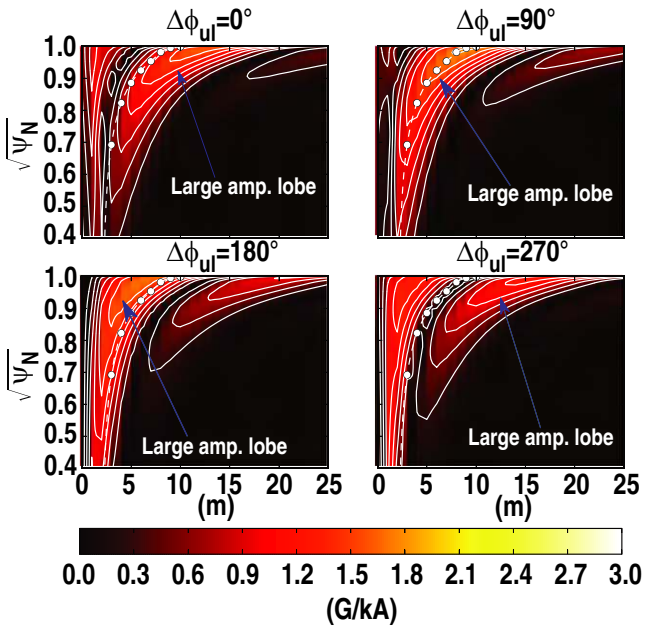

Figure 9. The applied vacuum field ($|\delta B^{m,n=2}_{r,\mathrm{vac}}(s)|$) for four discrete $\Delta\phi_{\mathrm{ul}}$ values, where $q_{95} = 3.9$ and $\beta_{\mathrm{N}}/\ell_{\mathrm{i}} = 2.0$. The pitch-resonant strength at the $m = nq$ harmonics (marked by white dots) varies considerably depending on $\Delta\phi_{\mathrm{ul}}$. The lobe of strong harmonics sweeps towards lower m as $\Delta\phi_{\mathrm{ul}}$ increases from 0° causing the ridge of maximum $|\delta B^{m,n=2}_{r,\mathrm{vac}}(s)|$ to sweep over the pitch-resonant harmonics, with a maximum in $\delta B^{n=2}_{\mathrm{res}}$ occurring near $\Delta\phi_{\mathrm{ul}} = 90°$. For $\Delta\phi_{\mathrm{ul}} = 270°$, the $m = nq$ line is in a valley and couples very poorly to the pitch-resonant harmonics.

drive. This is demonstrated in figure 9, where $\delta B^{m,n=2}_{r,\mathrm{vac}}(s)$ is shown for four separate $\Delta\phi_{\mathrm{ul}}$ values for an equilibrium with $q_{95} = 3.9$ and $\beta_{\mathrm{N}}/\ell_{\mathrm{i}} = 2.0$. As $\Delta\phi_{\mathrm{ul}}$ is increased from 0°, the lobe of strong harmonics moves towards the lower poloidal harmonics passing over the $m = nq$ resonances in the process. We can take advantage of the linearity of the MARS-F code to substantially reduce our computation requirements when calculating the dependence on $\Delta\phi_{\mathrm{ul}}$. In MARS-F it is possible to calculate the response to the upper array only (δB_{U}) and the lower array (δB_{L}) only. $\Delta\phi_{\mathrm{ul}}$ can then be taken into account by combining the two responses as follows: $\delta B_{\Delta\phi_{\mathrm{ul}}} = \delta B_{\mathrm{U}} + \delta B_{\mathrm{L}} \exp(\Delta\phi_{\mathrm{ul}}\mathrm{i})$. This represents a substantial computational saving and allows us to examine the $\delta B^{n=2}_{\mathrm{res}}$ dependence on q_{95} and $\Delta\phi_{\mathrm{ul}}$, while setting $\beta_{\mathrm{N}}/\ell_{\mathrm{i}} = 1.15$, without having to perform a new set of calculations for each $\Delta\phi_{\mathrm{ul}}$. The result is shown in figure 10. The regions of constant pitch-resonant drive essentially follow a straight line in ($\Delta\phi_{\mathrm{ul}}$, q_{95}) space. This result demonstrates how q_{95} and $\Delta\phi_{\mathrm{ul}}$ interact with one another to determine the efficiency of the coupling of $\delta B^{m,n=2}_{r,\mathrm{vac}}(s)$ to the pitch-resonant harmonics, with $\Delta\phi_{\mathrm{ul}}$ providing a more dominant contribution. There is also a general increase (decrease) in the maximum achievable $\delta B^{n=2}_{\mathrm{res}}$ ($\overline{\delta B}^{n=2}_{\mathrm{res}}$) as q_{95} increases, indicating that while an increase in q_{95} causes more resonant harmonics to be present in the plasma, the average amplitude of these harmonics decreases as q_{95} increases. This is ultimately due to the geometry of the MP coils, which restrict the range of accessible poloidal harmonics.

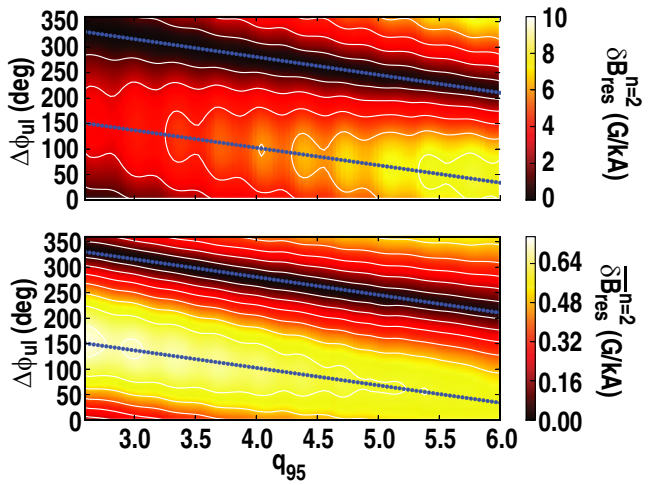

Figure 10. Measures of the pitch-resonant drive ($\delta B^{n=2}_{\mathrm{res}}$ and $\overline{\delta B}^{n=2}_{\mathrm{res}}$) plotted as a function of $\Delta\phi_{\mathrm{ul}}$ and q_{95}. The regions of maximum and minimum pitch-resonant drive follow nearly straight lines. Linear best fits to the maxima and minima are overlaid in blue. For any given q_{95} value, it is possible to achieve a large range in $\delta B^{n=2}_{\mathrm{res}}$ and $\overline{\delta B}^{n=2}_{\mathrm{res}}$ by varying $\Delta\phi_{\mathrm{ul}}$.

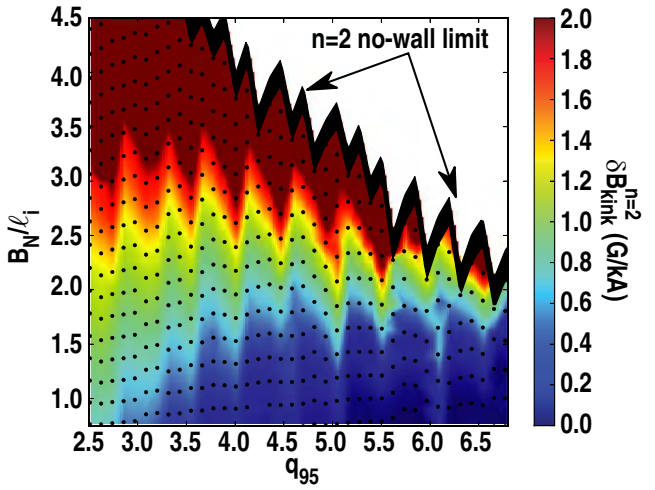

Figure 11. A measure of the kink-resonance, $\delta B^{n=2}_{\mathrm{kink}}$, calculated as a function of $\beta_{\mathrm{N}}/\ell_{\mathrm{i}}$ and q_{95} for $\Delta\phi_{\mathrm{ul}} = 0°$. There is a strong dependence on $\beta_{\mathrm{N}}/\ell_{\mathrm{i}}$ and a smaller periodic dependence on q_{95} due to low-n peeling modes. The thick black line marks the $n = 2$ no-wall limit.

4.2. Maps of kink resonance

The strength of the kink resonance depends strongly on $\Delta\phi_{\mathrm{ul}}$ and the plasma pressure (as measured by $\beta_{\mathrm{N}}/\ell_{\mathrm{i}}$) with a weaker dependence on the magnetic topology near the boundary (as measured by q_{95}). Figure 11 shows $\delta B^{n=2}_{\mathrm{kink}}$ calculated as a function of these parameters for $\Delta\phi_{\mathrm{ul}} = 0°$. The strong dependence on plasma pressure is expected because as the pressure is increased, the kink mode approaches instability causing a larger RFA. The dependence on q_{95} is more complicated, with periodic maxima occurring twice every half integer increase in q_{95}. This is due to the response from low-n peeling modes, which can also couple to the low-frequency/static, low-n MPs [38]. An important question, which is currently being investigated, is whether this instability

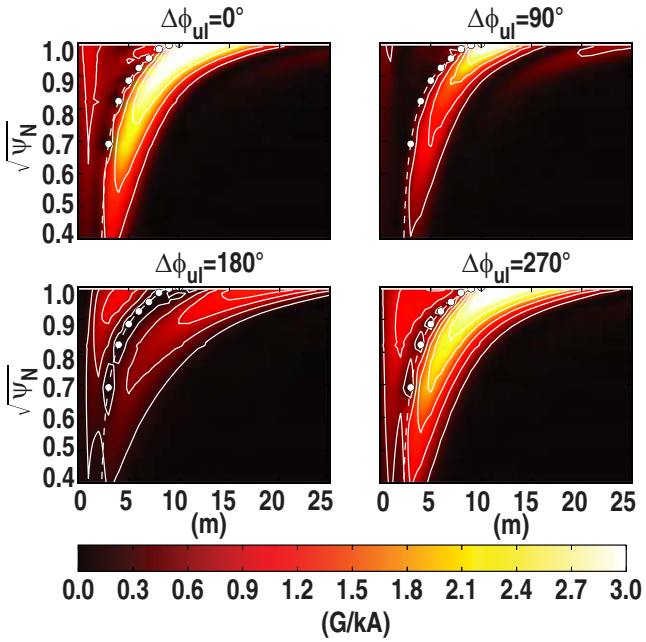

Figure 12. The vacuum field plus the plasma response ($|\delta B^{m,n=2}_{r,\mathrm{tot}}(s)|$) for the same equilibrium and $\Delta\phi_{\mathrm{ul}}$ values as figure 9. The amplitude of the harmonics $nq < m < 3nq$ vary considerably depending on $\Delta\phi_{\mathrm{ul}}$ with the strongest amplification occurring for 0° and 270° which are the cases where $|\delta B^{nq<m<3nq,n=2}_{r,\mathrm{vac}}(s)|$ is greatest. These images also show the nulls in the pitch-resonant harmonics (white dots) which are due to the ideal plasma response. These images have been smoothed over the discrete m to make trends easier to see.

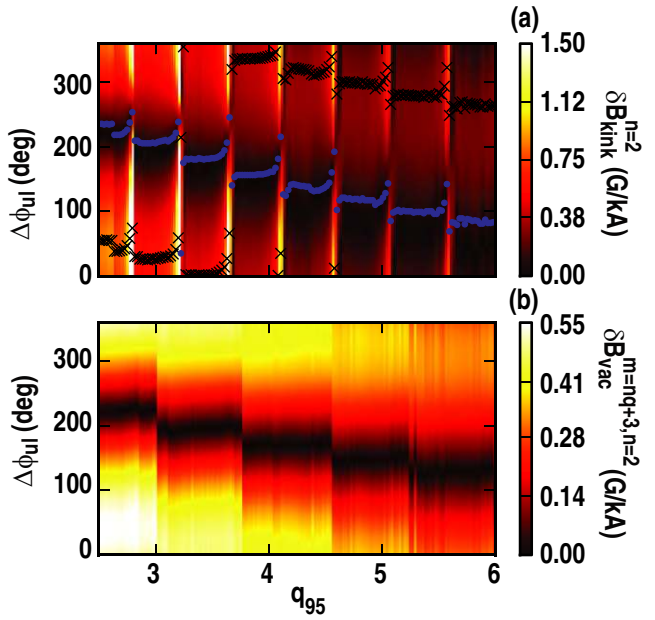

Figure 13. Plots of (*a*) $\delta B^{n=2}_{\mathrm{kink}}$ and (*b*) $\delta B^{m=nq+3,n=2}_{\mathrm{vac}}(s = 0.92)$ as a function of $\Delta\phi_{\mathrm{ul}}$ and q_{95}, with $\beta_{\mathrm{N}}/\ell_{\mathrm{i}} = 1.15$. The maxima and minima are marked by crosses and dots respectively. The location of the dots also marks the q_{95} values of the equilibria used for the calculations showing a dense sampling of q_{95} to capture the maxima.

is artificially induced by the finite edge q due to the flux truncation required by MARS-F (described in section 4), or if this is a physical result that would still occur if the x-point were included in the calculation.

As with the pitch-resonant component, varying $\Delta\phi_{\mathrm{ul}}$ significantly alters the vacuum poloidal spectrum causing large variations in the kink-resonant response. This is demonstrated in figure 12, where the same four $\Delta\phi_{\mathrm{ul}}$ values from figure 9 are used, except here $|\delta B^{m=nq,n}_{r,\mathrm{tot}}(s)|$ is shown to illustrate the contribution from the plasma response. Strong amplification occurs for $\Delta\phi_{\mathrm{ul}} = 0°$ and 270°, which are also the cases where $|\delta B^{nq<m<3nq,n=2}_{r,\mathrm{vac}}(s)|$ is greatest.

A harmonic in the edge vacuum magnetic field that satisfies $nq < m < 3nq$ can be used to provide a good first-order estimate of the kink response. This is shown in figure 13 where $\delta B^{n=2}_{\mathrm{kink}}$ (*a*) and $|\delta B^{m=nq+3,n=2}_{\mathrm{vac}}(s = 0.92)|$ (*b*) are plotted as a function of q_{95} and $\Delta\phi_{\mathrm{ul}}$, with $\beta_{\mathrm{N}}/\ell_{\mathrm{i}} = 1.15$. The trends in the two plots are similar, suggesting $|\delta B^{m=nq+3,n=2}_{\mathrm{vac}}(s = 0.92)|$ can be used as a first-order estimate of the kink resonance without calculating the plasma response.

The periodic maxima occurring twice every integer due to low-n peeling modes are a prominent feature in the measure of the kink response (figures 13(*a*) and 17). Here, substantially more artificial equilibria were used to more densely sample q_{95} to capture the periodic maxima (q_{95} is sampled in increments of ≈0.02). The maxima occur over a narrow q_{95} range of ≈0.1 and could be associated with the narrow q_{95} ELM suppression windows that have been observed [18, 48]. These periodic maxima are not captured in the vacuum calculation (figure 13(*b*)) and illustrate the importance of including the plasma response.

As with the pitch-resonant drive, the $\Delta\phi_{\mathrm{ul}}$ that gives the maximum kink-resonant response decreases slowly as q_{95} is increased, following an almost linear trend. Varying $\Delta\phi_{\mathrm{ul}}$ can change the kink resonance by more than an order of magnitude for the same q_{95} value, illustrating the utility of multi-row perturbation coils and the importance of including the plasma response.

4.3. Example uses of the pitch-resonant drive and kink-resonance maps

In this section, some examples are given that demonstrate how maps, like those shown in figures 10, 11 and 13, can be used to guide machine operations. It is possible to estimate the value of $\Delta\phi_{\mathrm{ul}}$, which maximizes the possibility of generating islands, or minimizes the excitation of the stable kink mode, for example. Additionally, these types of maps can be used for real-time control of $\Delta\phi_{\mathrm{ul}}$, and suggest that varying $\Delta\phi_{\mathrm{ul}}$ provides an effective method of testing the dependence of outcomes, such as ELM suppression, on pitch-resonant and kink-resonant drive. The experimentally observed $n = 2$ ELM suppression windows in [18] correspond to upper–lower I-coil phasings that maximize the kink-resonant response as opposed to the pitch-resonant response. This suggests that if one is looking for ELM suppression windows, the maps should be used to locate regions of strong kink-resonant forcing.

The maps allow $\Delta\phi_{\mathrm{ul}}$ to be optimized to achieve certain goals prior to an experiment. For example, if a shot is constrained such that $q_{95} = 3.5$, $\beta_{\mathrm{N}}/\ell_{\mathrm{i}} = 1.15$, and one wants to maximize (minimize) the possibility of generating islands,

then one could look for a maximum (minimum) in the applied pitch-resonant drive. The optimum $\Delta\phi_{ul} \approx 130^\circ(310^\circ)$ can be easily determined using figure 10. Alternatively, for the same shot, if a maximum (minimum) is required in the kink-resonant component, the optimum value of $\Delta\phi_{ul} \approx 10^\circ(190^\circ)$ can be calculated using figure 13. For the kink-resonant calculations, it is important to take β_N/ℓ_i into account, as this will play a critical role in the extent of the RFA; however, q_{95} and $\Delta\phi_{ul}$ determine the efficiency of the coupling of the MP to the kink-mode.

It is possible to achieve a substantial range of pitch-resonant drive and kink resonance for any given q_{95} by varying $\Delta\phi_{ul}$ (figures 10 and 13). This suggests that changing $\Delta\phi_{ul}$ throughout a shot provides an effective way of checking the effect of pitch-resonant drive, and kink resonance on experimental outcomes, such as ELM suppression. In [48], a q_{95} ramp-down was performed, which swept q_{95} across a resonant ridge in the poloidal mode number spectrum of the MP, to check for correlation with regions of ELM suppression. An alternative, is to sweep $\Delta\phi_{ul}$ and keep q_{95} fixed. This sweeps the poloidal mode number spectrum of the MP across the pitch-resonant harmonics (similar to what is shown in figure 12), allowing a larger range of pitch-resonant drive to be accessed. Additionally, this can be tried for any q_{95} value. Experimentally, sweeping the poloidal mode number spectrum of the MP across the pitch-resonant harmonics can be achieved by having a slight frequency difference between the upper MP array and the lower. If the frequency difference was 0.5 Hz, this would allow a rate of change in $\Delta\phi_{ul}$ of $180^\circ\,s^{-1}$. The rate of change in the phasing can be increased or decreased depending on the time available and the extent of the phasing window that one wants to examine. This idea is illustrated in figure 14 where, for $q_{95} = 3.5$ and $\beta_N/\ell_i = 1.15$, the normalized amplitudes of δB_{res} and $\delta B^{n=2}_{kink}$ are plotted as a function of $\Delta\phi_{ul}$, or time, if the perturbation in the lower array is slowly rotated as described above. Figure 14 clearly illustrates how effective $\Delta\phi_{ul}$ is at controlling the pitch-resonant (δB_{res}) and kink-resonant (δB_{kink}) components of the response.

The maps can also be used for real-time control of $\Delta\phi_{ul}$ to achieve a particular goal, such as maximizing the possibility of generating islands by maximizing the pitch-resonant drive throughout a shot. For example, as q_{95} varies throughout a shot, a real-time calculation of q_{95} can be used together with the relevant maps to change $\Delta\phi_{ul}$ to optimally align the ridge in the poloidal mode number spectrum of the MP with the pitch-resonant harmonics.

4.4. Relationship between pitch- and kink-resonant measures, and $n = 2$ ELM suppression

The narrow q_{95} ELM suppression windows (0.02, 0.06 and 0.2) that have been observed [18] are more consistent with the kink-resonant measure than the pitch-resonant measure. The pitch-resonant measure is quite smooth, and for any given q_{95} value, it is possible to achieve roughly the same level of pitch resonance by varying $\Delta\phi_{ul}$ (figure 10). On the other hand, the kink-resonant measure (figure 13) shows significant localized maxima in q_{95} due to a low-n peeling response.

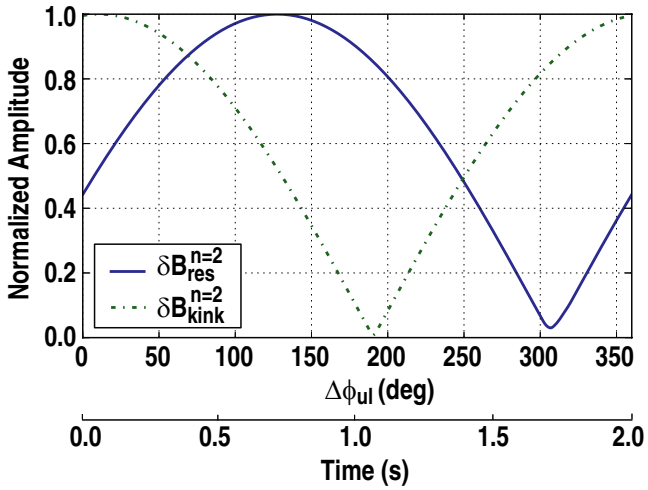

Figure 14. The $n = 2$ kink and pitch-resonant components ($\delta B^{n=2}_{kink}$ and $\delta B^{n=2}_{res}$) normalized to their maximum values plotted as a function of $\Delta\phi_{ul}$, or time, in a simulated experiment where the upper array has a $n = 2$ static MP, and the bottom array has a rotating 0.5 Hz $n = 2$ perturbation. Here, $q_{95} = 3.5$ and $\beta_N/\ell_i = 1.15$.

The width of these maxima is approximately 0.1 which is similar to the experimentally observed $n = 2$ ELM suppression windows. This suggests that the suppression of ELMs may be more closely related to the modified stability of global modes than with the creation of stochastic magnetic fields. However, it is important to point out that while the pitch-resonant measure is a good metric for how well the applied MP aligns with the resonant surfaces, it does not capture where the resonant surfaces are, or how they interact with one another, both of which will show a q_{95} dependence. Including these dependencies is the subject of future work. Additionally, because we are using the ideal MHD approximation, we are only looking at the vacuum field for the pitch-resonant measure. This does not capture the interplay between the stability of the global modes, and the pitch-resonant fields. A full two-fluid plasma response calculations with rotation and resistivity is necessary to more accurately calculate the pitch-resonant fields and confirm these results.

5. The importance of the n = 4 component in the dominantly n = 2 MP

In this section, we examine the importance of the $n = 4$ harmonic in the dominantly $n = 2$ MP. As was discussed in section 2, the $n \neq 2$ vacuum field harmonics are small, except for the $n = 4$ component. We show that the $n = 4$ pitch-resonant and kink-resonant components are substantially smaller than their $n = 2$ counterparts. Therefore, only considering the $n = 2$ component in the dominantly $n = 2$ MP provides a good approximation in most cases.

The $n = 2$ component of the pitch-resonant drive is substantially larger than the $n = 4$ component in most regions of parameter space. To measure the relative importance of $\overline{\delta B}^{n=2}_{res}$, figure 15 shows the proportion of the total drive caused by the $n = 2$ component ($\overline{\delta B}^{n=2}_{res}/(\overline{\delta B}^{n=2}_{res} + \overline{\delta B}^{n=4}_{res})$). This plot shows that $\overline{\delta B}^{n=2}_{res} \gg \overline{\delta B}^{n=4}_{res}$ in most regions of parameter

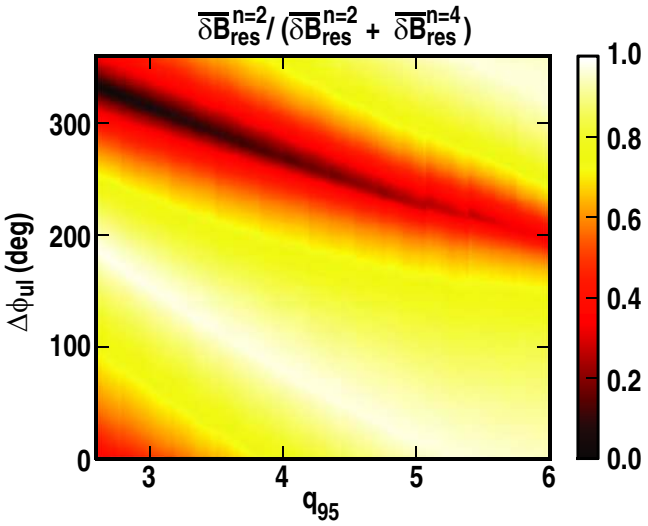

Figure 15. Proportion of the total pitch-resonant component caused by the dominant $n = 2$ harmonic as a function of $\Delta\phi_{ul}$ and q_{95}, showing the regions of parameter space where the $n = 4$ pitch-resonant component becomes significant.

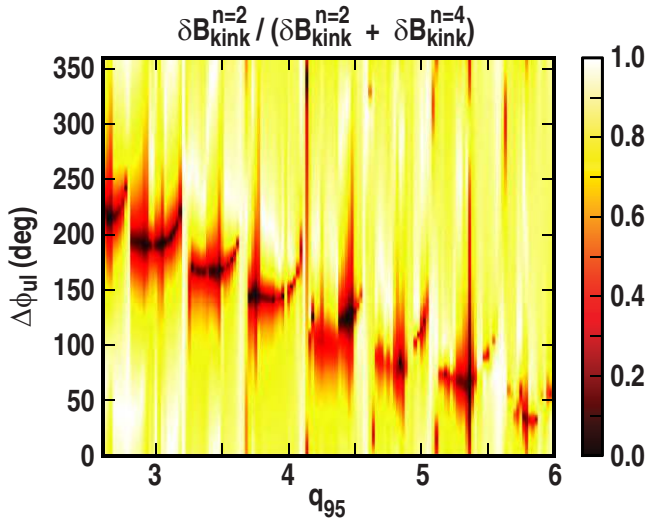

Figure 16. Proportion of the total kink-resonant component caused by the dominant $n = 2$ harmonic as a function of $\Delta\phi_{ul}$ and q_{95}, showing the regions of parameter space where the $n = 4$ kink-resonant component becomes significant.

space demonstrating that for the pitch-resonant response, the $n = 4$ component of the dominantly $n = 2$ MP can usually be ignored. In certain regions of parameter space where $\overline{\delta B}_{res}^{n=2}$ is small, $\overline{\delta B}_{res}^{n=4} > \overline{\delta B}_{res}^{n=2}$ indicating that the $n = 4$ component needs to be considered; however, the total pitch-resonant drive in these regions is still small. Another situation where the $n = 4$ component may be important is if one is considering island overlap between $n = 2$ and $n = 4$ islands. Note that the pitch-resonant drive calculation does not include the plasma response. If the resonant fields are amplified (for example due to an unstable tearing mode) for a particular equilibrium, this is not captured in these calculations.

As with pitch-resonant drive, the $n = 2$ component of the kink-resonant response is significantly larger than the $n = 4$ component. The proportion of the kink-resonant drive caused by the $n = 2$ component is shown in figure 16. This figure clearly illustrate that $\delta B_{kink}^{n=2} \gg \delta B_{kink}^{n=4}$ in most regions of parameter space. Additionally, $\delta B_{kink}^{n=2}$ and $\delta B_{kink}^{n=4}$, plotted as a function of q_{95} for $\Delta\phi_{ul} = 0^\circ$, are shown in figure 17 further demonstrating $\delta B_{kink}^{n=2} \gg \delta B_{kink}^{n=4}$ and highlighting the periodic maxima due to the low-n peeling modes. Therefore, we conclude that in most regions of parameter space, $\delta B_{kink}^{n=4}$ is substantially smaller than $\delta B_{kink}^{n=2}$ in the dominantly $n = 2$ MP.

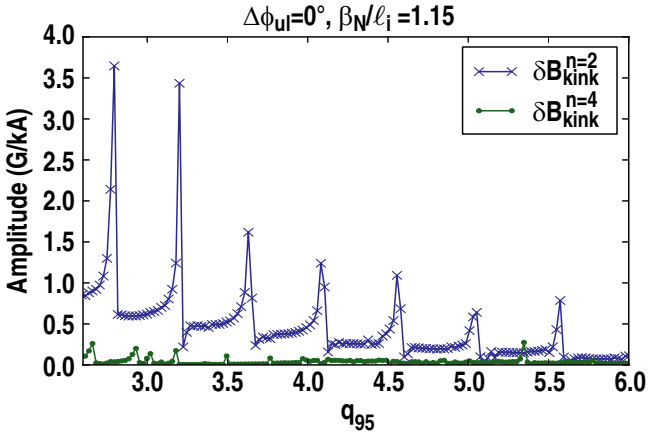

Figure 17. The $n = 2$ and $n = 4$ kink-resonant component ($\delta B_{kink}^{n=2}$ and $\delta B_{kink}^{n=4}$) as a function of q_{95}, with $\beta_N/\ell_i = 1.15$. The periodic maxima are due to the peeling response, and occur over narrow q_{95} ranges, which may be related to the narrow q_{95} ELM suppression regions.

6. Summary

An extensive examination of the $n = 2$ non-axisymmetric magnetic perturbation, as a function of $\Delta\phi_{ul}$ and plasma parameters on the DIII-D tokamak, using the linear MHD code MARS-F, has been presented. Pitch- and kink-resonant measures have been introduced and used to characterize the magnetic perturbations. These measures, while imperfect, represent an improvement on previous work on $n = 3$ perturbations [31] where a simulated magnetic probe response, and visual identification was used to separate out the responses.

Revisiting the $n = 3$ and other toroidal mode number perturbations on DIII-D, and the impact of the plasma response on $n = 3$ ELM suppression is the subject of future work. The $\Delta\phi_{ul}$ and plasma parameter dependence of pitch-resonant fields and the plasma kink-resonant response, have been mapped out, showing that $\Delta\phi_{ul}$ has a substantial influence on both of these responses. In many cases, $\Delta\phi_{ul}$ can have a larger effect than plasma parameters such as q_{95} and β_N/ℓ_i. This is of particular interest because $\Delta\phi_{ul}$ can be modified at will throughout a shot to achieve a desired effect provided sufficient power supplies are available.

The maxima and minima in the kink-resonant and pitch-resonant responses were found to follow an almost linear path in ($\Delta\phi_{ul}$, q_{95}) space, demonstrating how these two parameters interact to determine how efficiently the MP drives a pitch-resonant or kink-resonant response. Additionally, β_N/ℓ_i mainly determines the extent of the kink-resonant response.

Periodic increases in δB_{kink} are found twice for every integer increase in q_{95} due to low-n peeling modes. These periodic increases occur over small ranges in q_{95} suggesting that they could be related to the narrow, q_{95} ELM suppression windows that have been observed.

The separation of the plasma response into pitch-resonant and kink-resonant components is also useful for toroidal momentum confinement studies as these measures are related to the electromagnetic and NTV torque respectively. It should therefore be possible to use these measures to help determine under what plasma conditions and MP fields the electromagnetic or NTV torque will dominate. During such studies, it is critical to keep in mind the potential to indirectly increase the pitch-resonant harmonics by driving the kink mode, a key physics result observed in error field correction studies [15]. This will be the subject of future work.

The presence of other toroidal harmonics in the applied magnetic field was examined showing a substantial $n = 4$ component is present in the perturbations applied by the DIII-D I-coils. Examination of the plasma response to $n = 4$ perturbations shows that they are substantially smaller than the dominant $n = 2$ responses. This demonstrates that a good approximation to the dominantly $n = 2$ MP on DIII-D can be achieved using MARS-F and an idealized $n = 2$ MP.

The work presented here shows that a linear MHD code such as MARS-F can be used to effectively map out the plasma response dependence on plasma parameters and MP coil parameters such as dominant n and $\Delta\phi_{\text{ul}}$. These maps can then be used to guide real-time control of $\Delta\phi_{\text{ul}}$ to achieve specified outcomes, or alternatively decide on an optimum $\Delta\phi_{\text{ul}}$ in advance. Additionally, this type of approach can be used to optimize the design of MP coil sets.

Acknowledgments

This work was supported in part by the US Department of Energy under DE-FC02-04ER54698, DE-FG02-04ER54541 and DE-AC02-09CH11466. The authors wish to thank Drs A D Turnbull and M J Schaffer for several insightful discussions and the referee's for comments that helped clarify the ideas in this paper. SRH wishes to thank AINSE Ltd for providing financial assistance to enable this work to be conducted.

References

[1] Evans T E *et al* 2006 *Nature Phys.* **2** 419
[2] Evans T E *et al* 2008 *Nucl. Fusion* **48** 024002
[3] Evans T E *et al* 2004 *Phys. Rev. Lett.* **92** 235003
[4] Jeon Y M *et al* 2012 *Phys. Rev. Lett.* **109** 035004
[5] Suttrop W *et al* 2011 *Phys. Rev. Lett.* **106** 225004
[6] Liang Y *et al* 2007 *Phys. Rev. Lett.* **98** 265004
[7] Kirk A *et al* 2010 *Nucl. Fusion* **50** 034008
[8] Canik J M *et al* 2010 *Nucl. Fusion* **50** 034012
[9] Reimerdes H, Chu M S, Garofalo A M, Jackson G L, La Haye R J, Navratil G A, Okabayashi M, Scoville J T and Strait E J 2004 *Phys. Rev. Lett.* **93** 135002
[10] Shilov M *et al* 2004 *Phys. Plasmas* **11** 2573
[11] Okabayashi M *et al* 2005 *Nucl. Fusion* **45** 1715
[12] Cates C, Shilov M, Mauel M, Navratil G, Maurer D, Mukherjee S, Nadle D, Bialek J and Boozer A 2000 *Phys. Plasmas* **7** 3133
[13] La Haye R J *et al* 2002 *Phys. Plasmas* **9** 2051
[14] Garofalo A M, La Haye R J and Scoville J T 2002 *Nucl. Fusion* **42** 1335
[15] Park J-K, Schaffer M J, Menard J E, and Boozer A H 2007 *Phys. Rev. Lett.* **99** 195003
[16] Suttrop W *et al* 2009 *Fusion Eng. Des.* **84** 290
[17] Barlow I *et al* 2001 *Fusion Eng. Des.* **58** 189
[18] Lanctot M J *et al* 2013 *Nucl. Fusion* **53** 083019
[19] Lanctot M J *et al* 2010 *Phys. Plasmas* **17** 030701
[20] Turnbull A D 2012 *Nucl. Fusion* **52** 054016
[21] Nardon E *et al* 2011 *J. Nucl. Mater.* **415** S915–17
[22] Liu Y, Bondeson A, Fransson C, Lennartson B and Breitholtz C 2000 *Phys. Plasmas* **7** 3681
[23] Park W, Belova E V, Fu G Y, Tang X Z, Strauss H R and Sugiyama L E 1999 *Phys. Plasmas* **6** 1796
[24] Strauss H R *et al* 2009 *Nucl. Fusion* **49** 055025
[25] Ferraro N M and Jardin S 2009 *J. Comput. Phys.* **228** 7742
[26] Glasser A H, Sovinec C R, Nebel R A, Gianakon T A, Plimpton S J, Chu M S, Schnack D D and the NIMROD Team 1999 *Plasma Phys. Control. Fusion* **41** A747
[27] Izzo V A *et al* 2008 *Nucl. Fusion* **48** 115004
[28] Bécoulet M *et al* 2012 *Nucl. Fusion* **52** 054003
[29] Huysmans G and Czarny O 2007 *Nucl. Fusion* **47** 659
[30] Orain F *et al* 2013 *Phys. Plasmas* **20** 2510
[31] Lanctot M J *et al* 2011 *Phys. Plasmas* **18** 056121
[32] Liu Y, Kirk A, and Nardon E 2010 *Phys. Plasmas* **17** 122502
[33] Schaffer M J, Menard J, Aldan M, Bialek J, Evans T E and Moyer R A 2008 *Nucl. Fusion* **48** 024004
[34] Reimerdes H *et al* 2009 *Nucl. Fusion* **49** 115001
[35] Snyder P B *et al* 2012 *Phys. Plasmas* **19** 056115
[36] Liu Y *et al* 2012 *Plasma Phys. Control. Fusion* **54** 124013
[37] Garofalo A M, Jensen T H and Strait E J 2003 *Phys. Plasmas* **10** 4776
[38] Liu Y *et al* 2010 *Plasma Phys. Control. Fusion* **52** 045011
[39] Kirk A *et al* 2013 *Nucl. Fusion* **53** 043007
[40] Holcomb C *et al* 2006 *Rev. Sci. Instrum.* **77** 10E506
[41] Carlstrom T N *et al* 1992 *Rev. Sci. Instrum.* **63** 4901
[42] Burrell K H, Kaplan D, Gohil P, Nilson D, Groebner R J and Thomas D M 2001 *Rev. Sci. Instrum.* **72** 1028
[43] St John H E, Ferron J R, Lao L L, Osborne T H, Thompson S J and Wroblewski D 1994 *Proc. 15th Int. Conf. on Plasma Physics and Controlled Nuclear Fusion Research (Seville, Spain, 1994)* vol 3, p 603
[44] Lao L L, St John H E, Peng Q, Ferron J R, Strait E J, Taylor T S, Meyer W H, Zhang C and You K 2005 *Fusion Sci. Technol.* **48** 968
[45] Crotinger J, LoDestro L, Pearlstein L, Tarditi A, Casper T and Hooper E 1997 'Corsica: a comprehensive simulation of toroidal magnetic-fusion devices, Final Report to the LDRB Program *Technical Report* Lawrence Livermore National Laboratory, Livermore, CA
[46] Glasser A and Chance M S 1997 *Bull. Am. Phys. Soc.* **42** 1848
[47] Lutjens H, Bondeson A and Sauter O 1996 *Comput. Phys. Commun.* **97** 219
[48] Schmitz O *et al* 2009 *Phys. Rev. Lett.* **103** 165005